HARD BAINITE

H. K. D. H. Bhadeshia

University of Cambridge, Materials Science and Metallurgy
Pembroke Street, Cambridge CB2 3QZ, U. K.
www.msm.cam.ac.uk/phase–trans

Abstract

It is possible to create bainite in the form of long, slender crystals of ferrite whose scale compares with that of carbon nanotubes. These crystals are about 200Å in thickness and are generated by the partial transformation of austenite. The result is an extraordinary combination of strength and toughness; the bainite has the highest hardness and lowest transformation temperature ever reported. The mechanism of transformation is such that a stable carbon concentration which is many orders of magnitude greater than its equilibrium solubility, is retained in the ferrite in spite of aggressive tempering heat–treatments. All this can be achieved in bulk steel and without the use of expensive solutes, deformation or rapid thermal treatments. The science associated with this bainite is described, together with a series of characterisation experiments ranging from atoms to the behaviour of large components in violent deformation.

Introduction

The choreography of atoms during the course of the bainite transformation has major consequences on the development of structure at a variety of scales. In particular, the scale and extent of the structure is dependent directly on the fact that the atoms move in a disciplined fashion. This information can be exploited to develop unconventional alloys – for example, rail steels which do not rely on carbides for their properties, and the hardest ever bainite which can be manufactured in bulk form, without the need for rapid heat treatment or mechanical processing [1, 2, 3, 4, 5, 6, 7]. The purpose of this paper is to describe the current understanding of this novel hard bainite in terms of atomic mechanisms, thermodynamics and structure–property relationships.

The Limiting Transformation Temperature

What is the minimum temperature at which bainite can form? To answer this question requires a knowledge of the aomic mechanisms of nucleation and growth. However, any

calculation about bainite cannot be considered in isolation; for example, one limitation is that martensitic transformation must be avoided. We begin this discussion with a consideration of nucleation and then set out the general conditions rationalising the variety of solid–state transformations that occur in steels and which lead to an invariant–plane strain shape deformation with a large shear component. The discussion will rely on certain free energy changes which are explained first for clarity. This is followed by a brief explanation of how the displacive transformations in steels fit together in terms of nucleation and growth phenomena.

Thermodynamics

There is a significant change in the chemical composition of the austenite when it decomposes into the equilibrium mixture of ferrite and austenite. A ferrite nucleus on the other hand has such a small volume that it hardly affects the composition of the remaining austenite. The calculation of the free energy change associated with nucleation must therefore take into account that only a minute quantity of ferrite is formed. The free energy change for the formation of a mole of ferrite nuclei of composition x^α is given by ΔG_3, Fig. 1a [8, 9].
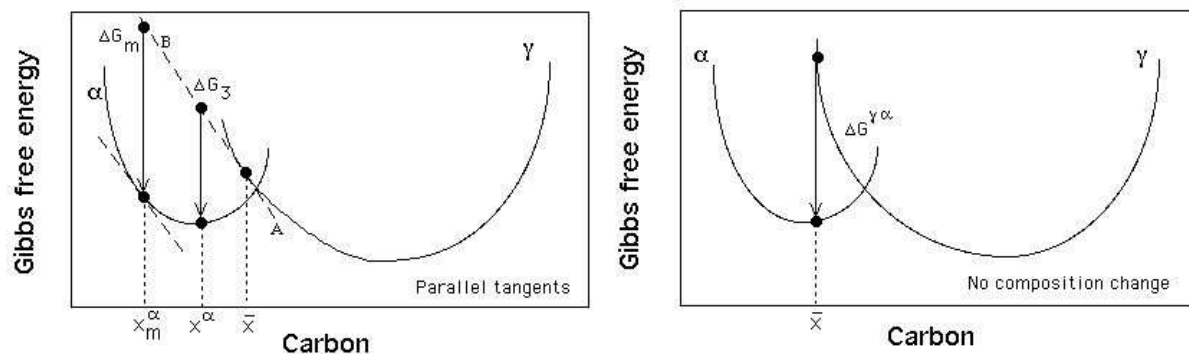
Figure 1: Free energy diagrams illustrating (a) the chemical free energy changes during the nucleation and (b) the growth of bainitic–ferrite from austenite of composition $\overline{x}$.

The greatest reduction in free energy during nucleation is obtained if the composition of the ferrite nucleus is set to a value x_m, given by a tangent to the ferrite free energy curve which is parallel to the tangent to the austenite free energy curve at $\overline{x}$, as shown in Fig. 1a. This maximum possible free energy change for nucleation is designated ΔG_m.

There is simplification when the transformation occurs without composition change (Fig. 1b). The change $\Delta G^{\gamma\alpha}$ is the vertical distance between the austenite and ferrite free energy curves at the composition of interest.

We shall henceforth use ΔG_m for the case where nucleation occurs by a paraequilibrium mechanism and $\Delta G^{\gamma\alpha}$ for cases where there is no change in composition on transformation.

Transformation–Start Temperature

It is a common observation that the Widmanstätten ferrite–start (W_S) and bainite–start (B_S) temperatures are more sensitive to the steel composition than is the Ae_3 equilibrium–temperature where the austenite first transforms to ferrite on cooling at an infinitely slow rate. This indicates that the influence of solutes on the nucleation of Widmanstätten ferrite and bainite is more than just thermodynamic, Fig. 2.
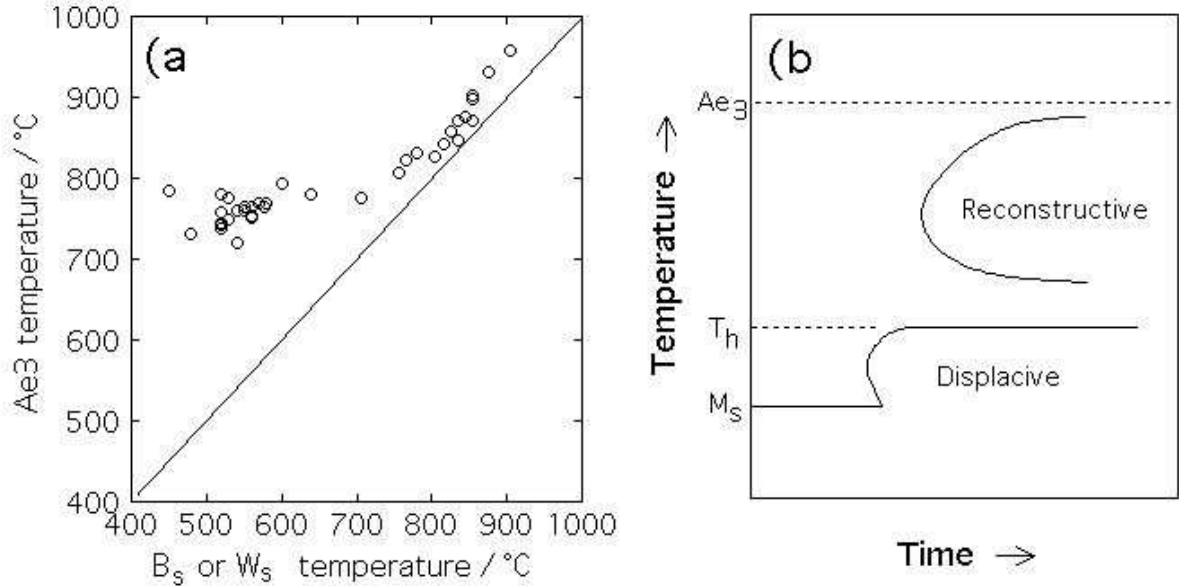
Figure 2: (a) The variation of the Widmanstätten ferrite–start and bainite–start temperatures as a function of the Ae_3 temperature of the steel concerned [10]. (b) Schematic TTT diagram illustrating the two C–curves and the T_h temperature.

Some clues to this behaviour come from studies of time–temperature–transformation diagrams, which consist essentially of two C–curves. The lower C–curve has a characteristic flat top at a temperature T_h, which is the highest temperature at which ferrite can form by displacive transformation, Fig. 2. The transformation product at T_h may be Widmanstätten ferrite or bainite.

The driving force ΔG_m available for nucleation at T_h, is plotted in Fig. 3a, where each point comes from a different steel. The transformation product at T_h can be Widmanstätten ferrite or bainite, but it is found that there is no need to distinguish between these phases for the purposes of nucleation. The same nucleus can develop into either phase depending on the prevailing thermodynamic conditions. The analysis proves that carbon must partition during the nucleation stage to provide the free energy required for nucleation. The situation illustrated in Fig. 3b is not viable since diffusionless nucleation would in some cases lead to an increase in the free energy.

The plots in Fig. 3 are generated using data from diverse steels. Fig. 3a represents the free energy change ΔG_m at the temperature T_h where displacive transformation first occurs. The free energy change can be calculated from readily available thermodynamic data. It follows that Fig. 3a can be used to estimate T_h for any steel. The equation fitted to the data
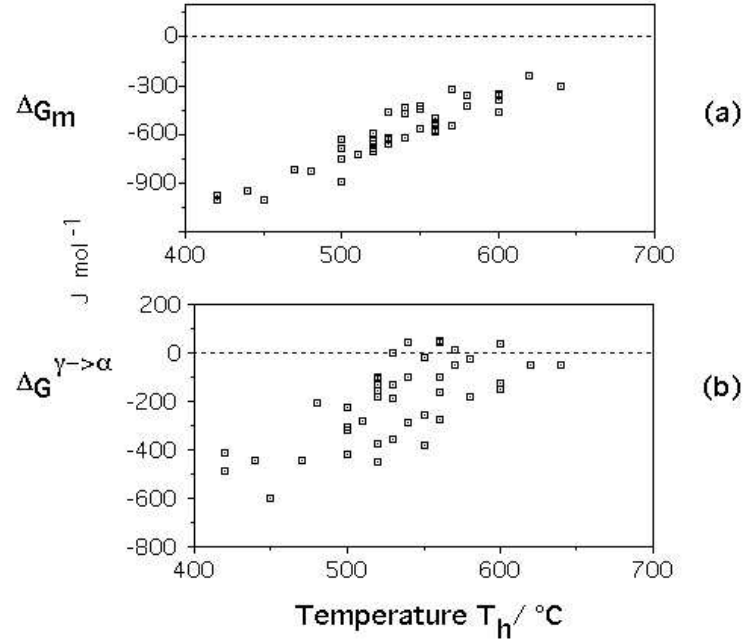
Figure 3: The free energy change necessary in order to obtain a detectable degree of transformation. Each point represents a different steel and there is no distinction made between Widmanstätten ferrite or bainite. (a) Calculated assuming the partitioning of carbon during nucleation. (b) Calculated assuming that there is no change in composition during nucleation. After Bhadeshia [8, 9].

in Fig. 3a is [8, 9, 11]:

$$G_N = C_1(T - 273.18) - C_2 \qquad \mathrm{J\,mol^{-1}} \tag{1}$$

where C_1 and C_2 are fitting constants for the illustrated temperature range. The linear relation between G_N and T is termed a *universal nucleation function*, because it defines the minimum driving force necessary to achieve a perceptible nucleation rate for Widmanstätten ferrite or bainite in any steel.

Evolution of the Nucleus

The nucleus is identical for Widmanstätten ferrite and for bainite; the transformations are distinguished by their growth mechanisms. But what determines whether the nucleus evolves into bainite or Widmanstätten ferrite?

The answer is straightforward. If diffusionless growth cannot be sustained at T_h then the nucleus develops into Widmanstätten ferrite so that T_h is identified with W_S. A larger undercooling is necessary before bainite can be stimulated. If, however, the driving force at T_h is sufficient to account for diffusionless growth, then $T_h = B_S$ and Widmanstätten ferrite does not form at all.

It follows that Widmanstätten ferrite forms below the Ae_3 temperature when:

$$\Delta G^{\gamma \rightarrow \gamma' + \alpha} < -G_{SW} \qquad \text{and} \qquad \Delta G_m < G_N \tag{2}$$

where G_{SW} is the stored energy of Widmanstätten ferrite (about 50 J mol^{-1}). $\Delta G^{\gamma \to \gamma' + \alpha}$ is the free energy change associated with the paraequilibrium growth of Widmanstätten ferrite [12]. The first of these conditions ensures that the chemical free energy change exceeds the stored energy of the Widmanstätten ferrite, and the second that there is a detectable nucleation rate.

Bainite is expected below the T_0' temperature when:

$$\Delta G^{\gamma \alpha} < -G_{SB} \qquad \text{and} \qquad \Delta G_m < G_N \tag{3}$$

where G_{SB} is the stored energy of bainite (about 400 J mol^{-1}). The universal function, when used with these conditions, allows the calculation of the Widmanstätten ferrite–start and bainite–start temperatures from a knowledge of thermodynamics alone.

In this scheme, carbon is partitioned during nucleation but in the case of bainite, not during growth which is diffusionless. There is no inconsistency in this concept since a greater fraction of the free energy becomes available as the particle surface to volume ratio, and hence the influence of interfacial energy, decreases.

The scheme is illustrated in Figure 4 which incorporates an additional function $G_N^{\alpha'}$ representing the critical driving force $\Delta G^{\gamma \to \alpha}\{M_S\}$ needed to stimulate martensite by an athermal, diffusionless nucleation and growth mechanism. Martensitic transformation occurs when $\Delta G^{\gamma \alpha}$ becomes less than a critical value $\Delta G^{\gamma \alpha}\{M_S\}$ given by the function $G_N^{\alpha'}$:

$$\Delta G^{\gamma \alpha} < G_N^{\alpha'} \tag{4}$$

Whereas it is reasonable to set $G_N^{\alpha'}$ to an approximately constant value for low–alloy steels [14, 15, 16, 17] a function dependent on the strength of the austenite has to be used for steels containing large concentrations of solute [18].

The scheme is illustrated in Fig. 4. It explains why bainite and martensite do not form in every steel. Consider steel **b** in Fig. 4, which contains a larger concentration of austenite stabilising elements than steel **a**. Therefore, whereas the conditions outlined in equations 3 and 4 lead to both bainite and martensite in steel **a**, the point where bainite formation becomes possible in steel **b** is also the M_S temperature. Since martensite has a huge kinetic advantage over bainite, the latter is absent in steel **b**. Thus, for example, only martensite occurs in Fe–28Ni–0.4C wt%, whereas both bainite and martensite are found in Fe–4Cr–0.3C wt%.

The Mechanism of Nucleation

The universal function G_N was originally derived by fitting to experimental data over the temperature range 400–650°C [8, 11] and has been demonstrated more recently for high–carbon steels [19]. It is nevertheless empirical and requires some justification for the linear dependence of G_N on T_h (Fig. 4) before it can be extrapolated to explore low transformation temperatures and address the question about the minimum temperature at which bainite can be obtained.

Classical nucleation theory involving hetrophase fluctuations is not appropriate for bainite [9] given that thermal activation is in short supply. Furthermore, it leads to a relationship
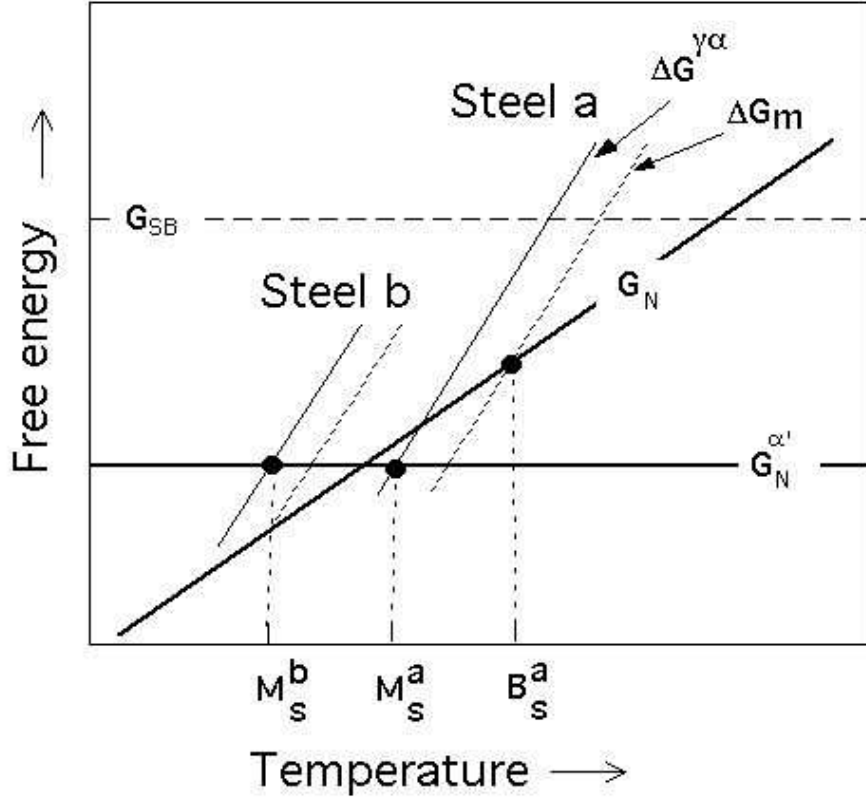
Figure 4: Free energy curves of low (a) and high (b) alloy steel showing the conditions necessary for the nucleation and growth of bainite and martensite.

between the chemical driving force ΔG_{CHEM} and the activation energy G^* for nucleation as

$$G* \propto \Delta G_{CHEM}^{-2} \tag{5}$$

which cannot explain the proportionality between G_N and T_h [9].

One mechanism in which the barrier to nucleation becomes sufficiently small involves the spontaneous dissociation of specific dislocation defects in the parent phase [20, 21]. The dislocations are glissile so the mechanism does not require diffusion. The only barrier is the resistance to the glide of the dislocations. The nucleation event cannot occur until the undercooling is sufficient to support the faulting and strains associated with the dissociation process that leads to the creation of the new crystal structure.

The free energy per unit area of fault plane is:

$$G_F = n_P \rho_A (\Delta G_{CHEM} + G_{STRAIN}) + 2\sigma_{\alpha\gamma}\{n_P\} \tag{6}$$

where n_P is the number of close–packed planes participating in the faulting process, ρ_A is the spacing of the close–packed planes on which the faulting is assumed to occur. The fault energy can become negative when the austenite becomes metastable.

For a fault bounded by an array of n_P dislocations each with a Burgers vector of magnitude b, the force required to move a unit length of dislocation array is $n_P \tau_o b$. τ_o is the shear resistance of the lattice to the motion of the dislocations. G_F provides the opposing

stress via the chemical free energy change ΔG_{CHEM}; the physical origin of this stress is the fault energy which becomes negative so that the partial dislocations bounding the fault are repelled. The defect becomes unstable, *i.e.,* nucleation occurs, when

$$G_F = -n_P\tau_o b \tag{7}$$

Take the energy barrier between adjacent equilibrium positions of a dislocation to be G_o^*. An applied shear stress τ has the effect of reducing the height of this barrier [22, 23]:

$$G^* = G_o^* - (\tau - \tau_\mu)v^* \tag{8}$$

where v^* is an activation volume and τ_μ is the temperature independent resistance to dislocation motion. In the context of nucleation, the stress τ is not externally applied but comes from the chemical driving force. On combining the last three equations we obtain [21]:

$$G^* = G_o^* + \left[\tau_\mu + \frac{\rho_A}{b}G_{STRAIN} + \frac{2\sigma}{n_P b}\right]v^* + \frac{\rho_A v^*}{b}\Delta G_{CHEM} \tag{9}$$

It follows that with this model of nucleation the activation energy G^* will decrease *linearly* as the magnitude of the driving force ΔG_{CHEM} increases. This direct proportionality contrasts with the inverse square relationship of classical theory.

The nucleation rate I_V will have a temperature dependence due to the activation energy:

$$I_V \propto \nu \exp\{-G^*/RT\} \tag{10}$$

where ν is an attempt frequency. It follows that

$$-G^* \propto \beta T \qquad \text{where} \qquad \beta = R\ln\{I_V/\nu\} \tag{11}$$

We now assume that there is a specific nucleation rate at T_h, irrespective of the type of steel, in which case β is a constant, negative in value since the attempt frequency should be larger than the actual rate. This gives the interesting result that

$$G_N \propto \beta T \tag{12}$$

which is precisely the relationship observed experimentally, Fig. 3a. This is evidence for nucleation by the dissociation of dislocations with the activation energy proportional to the driving force, as opposed to the inverse square relationship predicted by classical theory. The activation energy G^* in this model comes from the resistance of the lattice to the motion of dislocations.

Nucleation corresponds to a point where the slow, thermally activated migration of glissile partial dislocations gives way to rapid, breakaway dissociation. This is why it is possible to observe two sets of transformation units, the first consisting of very fine embryo platelets below the size of the operational nucleus, and the second the size corresponding to the rapid growth to the final size. Intermediate sizes are rarely observed because the time period for the second stage is expected to be much smaller than that for the first. Figure 5 shows that in addition to the fully growth sub–units (a few micrometers in length), there is another population of much smaller (submicron) particles which represent the embryos at a point in their evolution prior to breakaway.
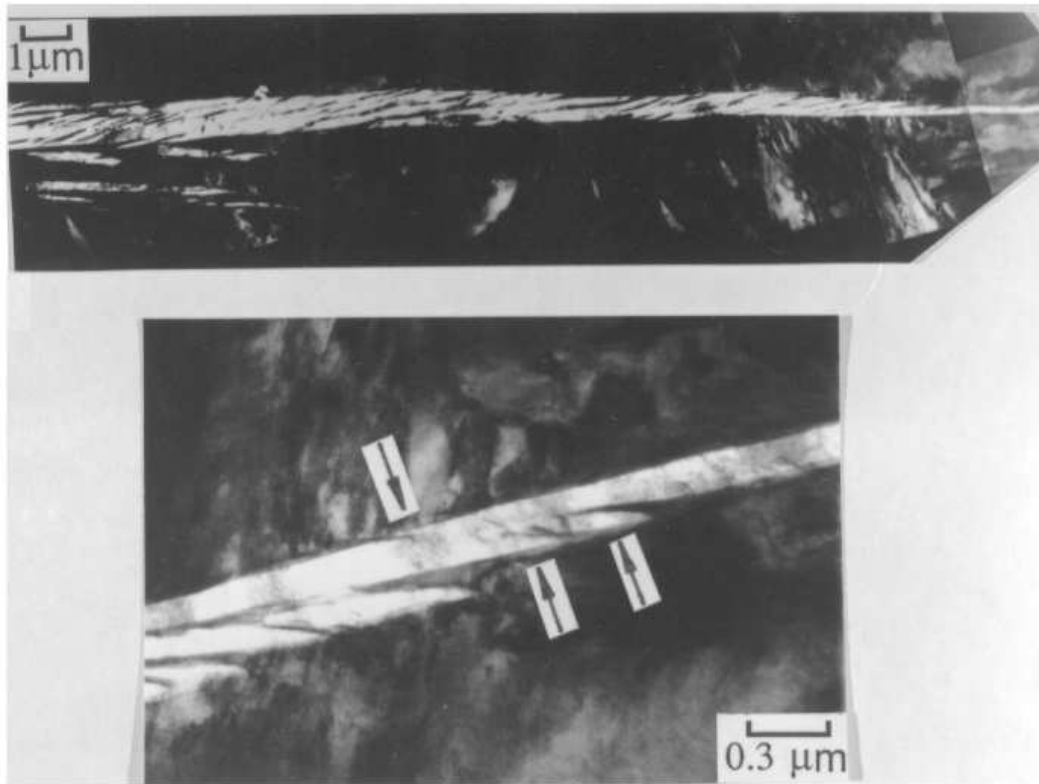
Figure 5: Transmission electron micrograph of a sheaf of bainite in a partially transformed sample. A region near the tip of the sheaf in (a) is enlarged in (b). The arrows in (b) indicate possible sub–operational embryos which are much smaller than the fully grown sub–units seen in (a). After [24]

Mechanism of Growth

In the absence of carbide precipitation, the bainite reaction stops when the driving force for diffusionless growth is exhausted. This and other observations lead to the conclusion that the individual platelets growth without diffusion, and that the carbon subsequently partitions into the residual austenite [25, 26, 27, 28, 29]

The scale of individual plates of bainitic ferrite is too small to be resolved adequately using optical microscopy, which is capable only of revealing clusters of plates. Using higher resolution techniques such as photoemission electron microscopy it has been possible to study directly the progress of the bainite reaction. Not surprisingly, the lengthening of individual bainite platelets has been found to occur at a rate which is much faster than expected from a diffusion–controlled process. The growth rate is nevertheless much smaller than that of martensite, because of the plasticity associated with the accommodation of the invariant–plane strain shape change. The platelets tend to grow at a constant rate but are usually stifled before they can traverse the austenite grain.

The complete scheme which describes the atomic mechanisms of solid–state transformations from austenite has been elaborated elsewhere [9, 28], but Table 1 summarises the essential details for Widmanstätten ferrite, bainite and martensite. These are some of the details which permit alloy design.

Table 1: Mechanisms of Displacive Transformations

Martensite α'	Bainite α_b	Widmanstätten ferrite α_W
Diffusionless nucleation	Paraequilibrium nucleation	Paraequilibrium nucleation
Diffusionless growth	Diffusionless growth	Paraequilibrium growth

Design

Suppose we now attempt to calculate the lowest temperature at which bainite can be induced to grow. As explained above, we have the theory to address this proposition. Such calculations are illustrated in Figure 6a, which shows for an example steel, how the bainite-start (B_S) and martensite-start (M_S) temperatures vary as a function of the carbon concentration. There is in principle no lower limit to the temperature at which bainite can be generated. On the other hand, the rate at which bainite forms slows down drastically as the transformation temperature is reduced, as shown by the calculations in Figure 6b. It may take hundreds or thousands of years to generate bainite at room temperature. For practical purposes, a transformation time of tens of days is reasonable. But why bother to produce bainite at a low temperature?
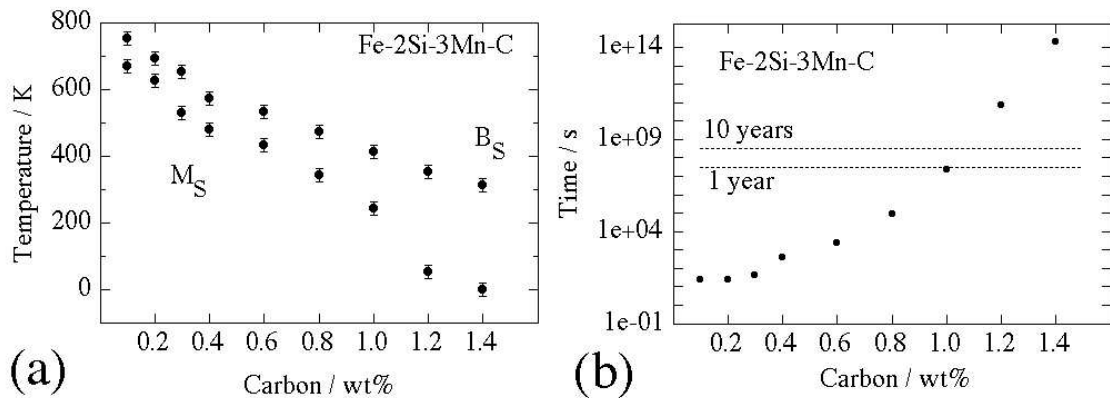
Figure 6: (a) Calculated transformation start temperatures in Fe-2Si-3Mn steel as a function of the carbon concentration. (b) The calculated time required to initiate bainite [13].

It is well known that the scale of the microstructure, *i.e.,* the thickness of the bainite plates, decreases as the transformation temperature is reduced. This is because the yield strength of the austenite becomes greater at lower temperatures, thereby affecting the plastic accommodation of the shape deformation accompanying bainite growth, and presumably because the nucleation rate can be greater at larger undercoolings. The strength of the microstructure scales with the inverse of the plate thickness, thus providing a neat way of achieving strength without compromising toughness.

Experiments consistent with the calculations illustrated in Figure 6 demonstrated that in a Fe-1.5Si-2Mn-1C wt% steel, bainite can be generated at a temperature as low at 125°C, which is so low that the diffusion distance of an iron atom is an inconceivable 10^{-17} m over the time scale of the experiment!

What is even more remarkable is that the plates of bainite are only 200–400 Å thick. The slender plates of bainite are dispersed in stable carbon–enriched austenite which, with its face–centred cubic lattice, buffers the propagation of cracks. The optical and transmission electron microstructures are shown in Fig. **??**; they not only have metallurgical significance in that they confirm calculations, but also are elegant to look at. Indeed, the microstructure has now been characterised, both chemically and spatially to an atomic resolution; the pleasing aesthetic appearance is maintained at all resolutions. There is no redistribution of substitutional atoms on the finest conceivable scale [30].

Ultimate tensile strengths of 2500 MPa in tension have been routinely obtained, ductilities in the range 5-30% and toughness in excess of 30-40 MPa m$^{1/2}$. All this in a dirty steel which has been prepared ordinarily and hence contains inclusions and pores which would not be there when the steel is made by any respectable process. The bainite is also the hardest ever achieved, 700 HV. The simple heat treatment involves the austenitisation of a chunk of steel (say 950°C), gently transferring into an oven at the low temperature (say 200°C) and holding there for ten days or so to generate the microstructure. There is no rapid cooling – residual stresses are avoided. The size of the sample can be large because the time taken to reach 200°C from the austenitisation temperature is much less than that required to initiate bainite. This is a major commercial advantage [31].

It is cheap to heat treat something at temperatures where pizzas are normally cooked. But suppose there is a need for a more rapid process. The transformation can easily be accelerated to occur within hours, by adding solutes which decrease the stability of austenite. There are two choices, aluminium and cobalt, in concentrations less than 2 wt%, have been shown to accelerate the transformation in the manner described. Both are effective, either on their own or in combination [32].

Much of the strength and hardness of the microstructure comes from the very small thickness of the bainite plates. Of the total strength of 2500 MPa, some 1600 MPa can be attributed solely to the fineness of the plates. The residue of strength comes from dislocation forests, the strength of the iron lattice and the resistance to dislocation motion due to solute atoms. Because there are many defects created during the growth of the bainite [9], a large concentration of carbon remains trapped in the bainitic ferrite and refuses to precipitate, probably because it is trapped at defects [**?**].

Strong Bainite: Armour

Whereas the ordinary tensile strength of the strong bainite is about 2.5 GPa, the strength has been reported to be as high as 10 GPa at the very high strain rates ($10^7 \, \text{s}^{-1}$) associated with ballistic tests [33].

The strong bainite has therefore found application in armour [34, 35]. Fig. 9 shows a series of tests conducted using projectiles which are said to involve "the more serious battlefield tests" (the details are proprietary). Figs. 9a,b show experiments in which an armour *system* is tested. A 12 mm thick sample of the bainitic steel is sandwiched between vehicle steel, the whole contained in glass–reinforced plastic. In ordinary armour the projectile would have penetrated completely whereas the bainite has prevented this; the steel did however crack. By reducing the hardness (transforming at a higher temperature), it was possible for the armour to support multiple hits (Fig. 9c) without being incorporated in an armour–system.
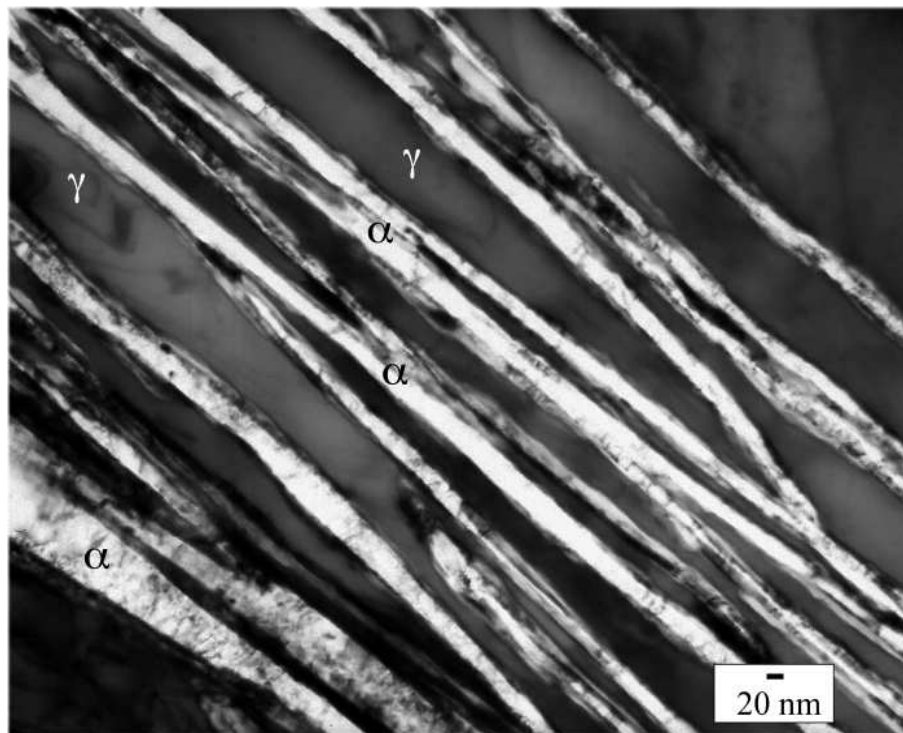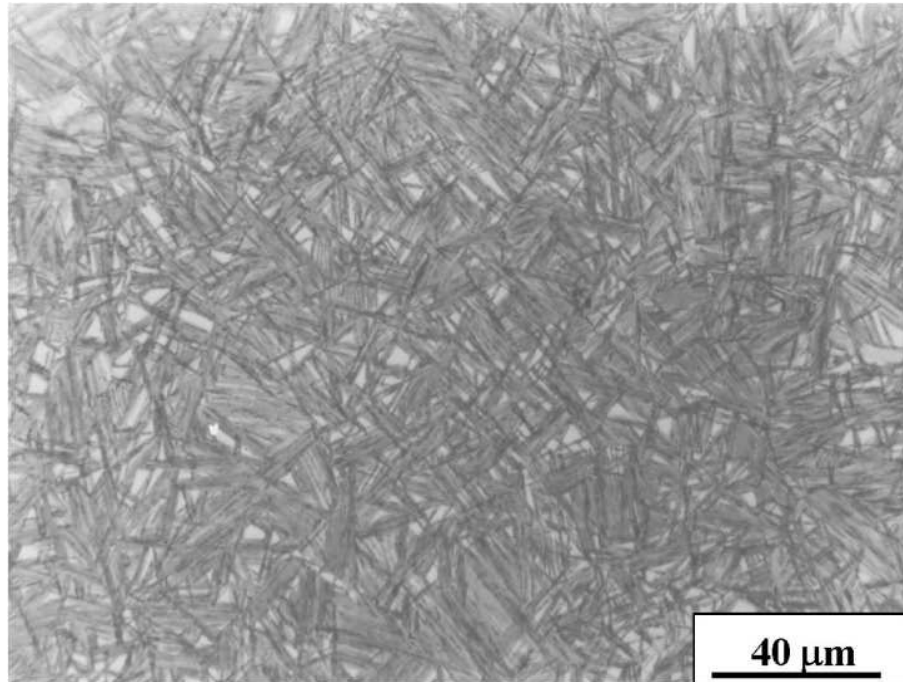
Figure 7: Fe-0.98C-1.46Si-1.89Mn-0.26Mo-1.26Cr-0.09V wt%, transformed at 200°C for 5 days. (a) Optical micrograph. (b) Transmission electron micrograph. [1, 2, 3]
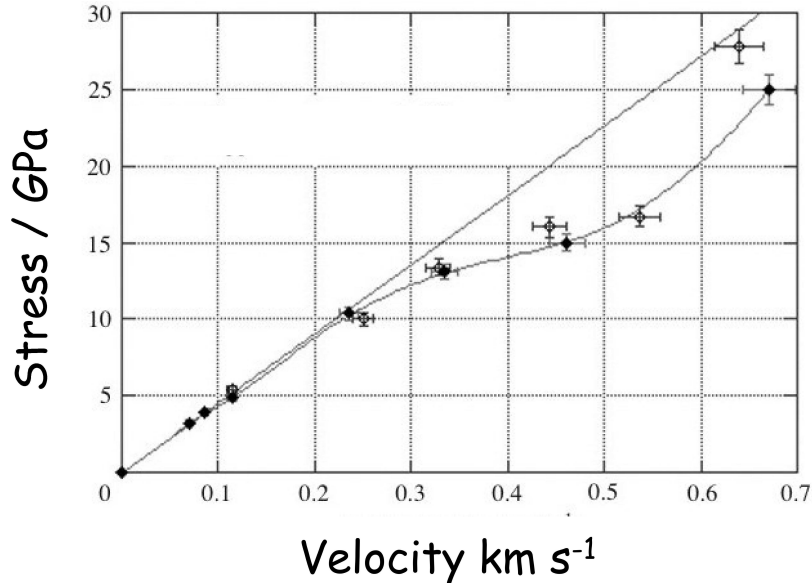
Figure 8: Ballistic test on the bainitic armour alloys [33]. Departure from the straight line indicates plasticity and the horizontal axis represents projectile velocity.

The ballistic mass efficiency BME of an armour is defined as

$$BME = \frac{\text{mass of ordinary armour to defeat a given threat}}{\text{mass of test armour to defeat same threat}} \qquad (13)$$

Fig. 9d shows that the BME of the strong bainite exceeds titanium armour and compares with the alumina [34].

Low–Carbon Hard Bainite?

High–carbon steels are difficult to weld because of the formation of untempered, brittle martensite in the coarse–grained heat–affected zones of the joints. The martensite fractures easily, leading to a gross deterioration in the structural integrity of the joint. For this reason, the vast majority of weldable steels have low carbon concentrations. It would be desirable therefore to make the low–temperature bainite with a much reduced carbon concentration.

Calculations done using the scheme outlined in this paper indicate that carbon is much more effective in maintaining a difference between the M_S and B_S temperatures than are substitutional solutes which reduce $|\Delta G^{\gamma\alpha}|$ simultaneously for martensite and bainite, Fig. 10. Substitutional solutes do not partition during any stage in the formation of martensite or bainite; both transformations are therefore identically affected by the way in which the substitutional solute alters the thermodynamic driving force. It is the partitioning of carbon at the nucleation stage which is one of the distinguishing features of bainite when compared with martensite (Table 1). This carbon partitioning allows bainite to form at a higher temperature than martensite. This advantage is diminished as the overall carbon concentration is reduced, as illustrated in Figure 10.

From these results, it must be concluded that it is not possible to design low–temperature bainite with a low carbon concentration.
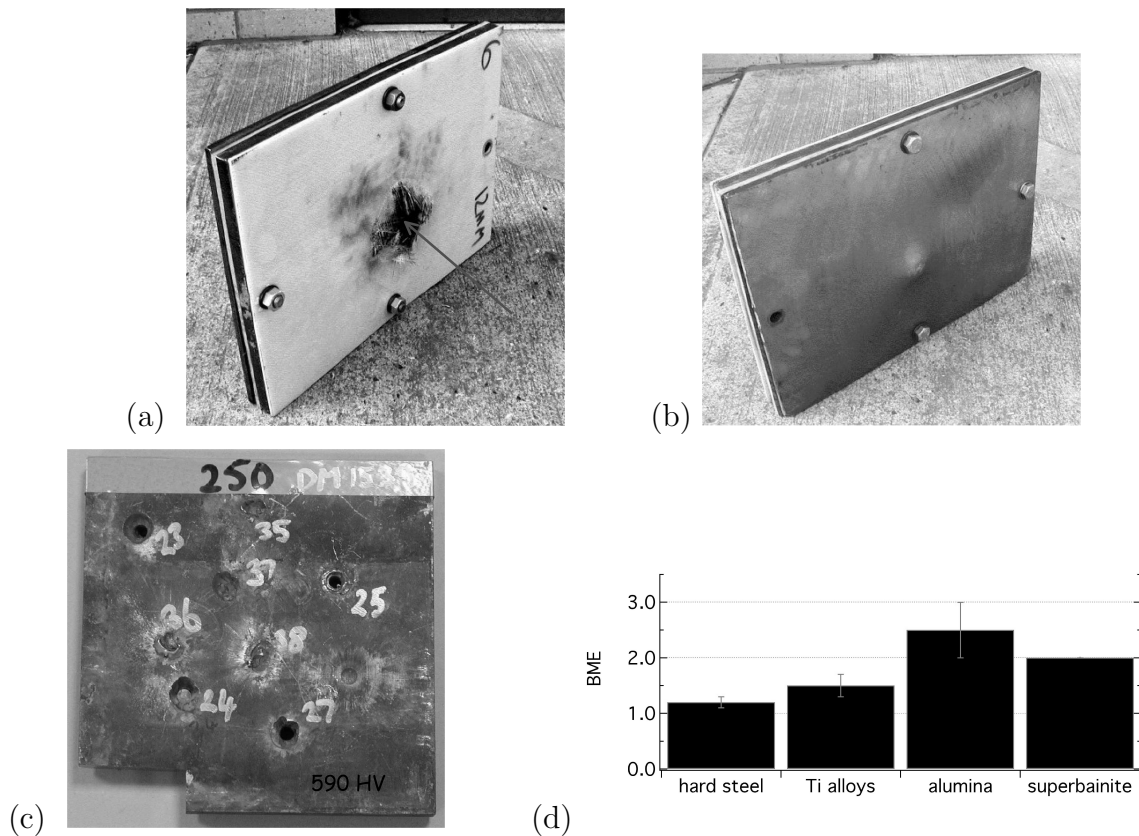
Figure 9: Fe-0.98C-1.46Si-1.89Mn-0.26Mo-1.26Cr-0.09V wt%, transformed at 200°C for 5 days. (a) 12 mm thick sample of bainite between two plates of ordinary vehicle armour, with a layer of glass–reinforced plastic. Arrow indicates the path of the projectile. (b) Rear view, showing lack of penetration. (c) Lower hardness bainitic armour - remains intact following multiple hits. (d) Comparison of armours. After D. Crowther and P. Brown.

Summary

There are many adjectives that have been given to the fine bainitic microstructure described in this paper:

- Cold-bainite because of the low temperatures at which it grows.

- Hard-bainite because the hardness of the microstructure (600–700 HV) almost matches that of the hardest untempered martensite.

- Strong–bainite because of the observed tensile strength (compressive strengths in excess of 4.5 GPa have been recorded, and tensile strength approaching 10 GPa at high strain rates).

- Fast–bainite for the faster transforming cobalt– and aluminium–containing variants [4].

- Super–bainite, an unfortunate term coined in industry.

There remain, as is always the case, many parameters which have yet to be characterised, for example the fatigue and stress-corrosion properties. However, this is work in progress
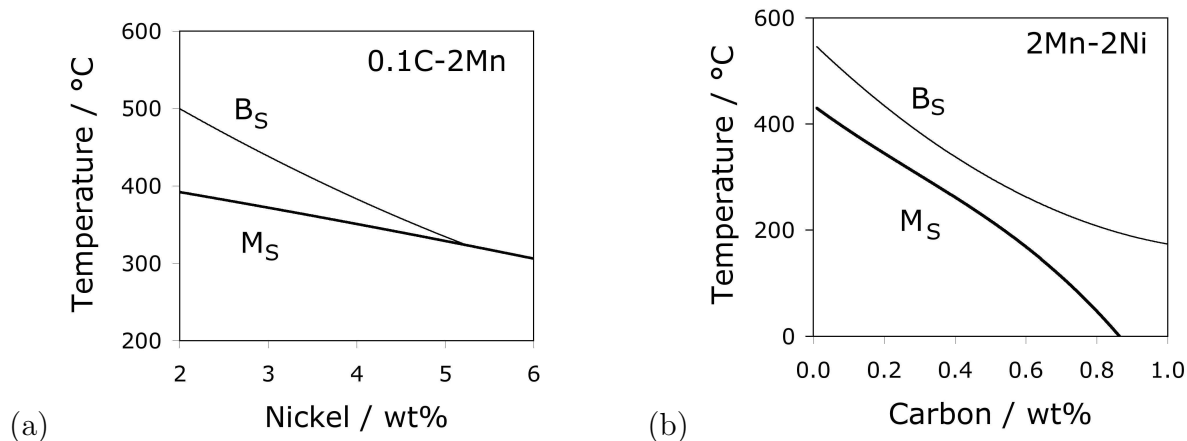
Figure 10: Calculated bainite and martensite–start temperatures: (a) Fe–0.1C–2Mn wt%, with a variation in nickel concentration; (b) Fe–2Ni–2Mn with a variation in the carbon concentration.

and is certainly not holding back the application of this alloy, which is a tribute to phase transformation theory.

Acknowledgments

References

[1] F. G. Caballero, H. K. D. H. Bhadeshia, K. J. A. Mawella, D. G. Jones and P. Brown, "Very Strong, Low–Temperature Bainite", *Materials Science and Technology*, 18 (2002) 279–284.

[2] C. Garcia–Mateo, F. G. Caballero, H. K. D. H. Bhadeshia, "Low Temperature Bainite", *Journal de Physique Colloque*, 112 (2003) 285–288.

[3] C. Garcia–Mateo, F. G. Caballero, H. K. D. H. Bhadeshia, "Hard Bainite", *ISIJ International*, 43 (2003) 1238–1243.

[4] C. Garcia–Mateo, F. G. Caballero, H. K. D. H. Bhadeshia, "Acceleration of Low–Temperature Bainite", *ISIJ International*, 43 (2003) 1821–1825.

[5] M. Peet, C. Garcia–Mateo, F. G. Caballero and H. K. D. H. Bhadeshia, "Tempering of a Hard Mixture of Bainitic Ferrite and Austenite", *Materials Science and Technology*, 20 (2004) 814–818.

[6] M. Peet, S. S. Babu, M. K. Miller and H. K. D. H. Bhadeshia, "Three-dimensional Atom Probe Analysis of Carbon Distribution in Low-Temperature Bainite", *Scripta Materialia*, 50 (2004) 1277–1281.

[7] F. G. Caballero and H. K. D. H. Bhadeshia, "Very Strong Bainite", *Current Opinion in Solid State and Materials Science,* 8 (2004) 251–257.

[8] H. K. D. H. Bhadeshia, "Rationalisation of Shear Transformations in Steels", *Acta Metallurgica,* 29 (1981), 1117–1130.

[9] H. K. D. H. Bhadeshia, *Bainite in Steels* (2nd edition, IOM Communications Ltd., London, 2001).

[10] Ali, A., "Widmanstatten ferrite and Bainite in Ultra–High Strength Steels", *Ph.D. Thesis*, University of Cambridge (1990).

[11] Ali, A. and Bhadeshia, H. K. D. H., "Aspects of the Nucleation of Widmanstätten ferrite", *Materials Science and Technology* 6 (1990) 781–784.

[12] Bhadeshia, H. K. D. H., "Critical Assessment: Diffusion–controlled Growth of Ferrite Plates in Plain Carbon Steels", *Materials Science and Technology,* 1 (1985) 497–504.

[13] H. K. D. H. Bhadeshia, "Thermodynamic Analysis of Isothermal Transformation Diagrams", *Metal Science,* 16 (1982) 159–165.

[14] L. Kaufman and M. Cohen, Thermodynamics and Kinetics of Martensitic Transformation, *Progress in Metal Physics,* 7 (1958) 165–246.

[15] Y. Imai, M. Izumiyama and M. Tsuchiya, "Thermodynamic Study on the Transformation of Austenite into Martensite in Fe–N and Fe–C systems", *Scientific Reports: Res. Inst. Tohoku University,* A17 (1965) 173–192.

[16] H. K. D. H. Bhadeshia, "The Driving Force for Martensitic Transformation in Steels", *Metal Science,* 15 (1981) 175–177.

[17] H. K. D. H. Bhadeshia, "Thermodynamic Extrapolation and the Martensite-Start Temperature of Substitutionally Alloyed Steels" *Metal Science* 15 (1981) 178–180.

[18] G. Ghosh and G. B. Olson, "Computational Thermodynamics and Kinetics of Martensitic Transformation", *Journal of Phase Equilibria,* 22 (2001) 199–207.

[19] Mateo, C. G. and Bhadeshia, H. K. D. H., "Nucleation Theory for High–Carbon Bainite", *Materials Science and Engineering A* 378A (2004) 289–292.

[20] Christian, J. W., "A Theory for the Transformation in Pure Cobalt", *Proc. Royal Society,* 206A (1951) 51–64.

[21] Olson, G. B. and Cohen, M., "A general mechanism for martensitic nucleation", *Metallurgical Transactions,* 7A (1976) 1897–1923.

[22] Conrad, H., "Thermally activated deformation of metals", *Journal of Metals,* July (1964) 582–588.

[23] Dorn, J. E., "Dislocation Dynamics", eds. A. R. Rosenfield, G. T. Hahn, A. L. Bement and R. I. Jaffee, McGraw–Hill, New York (1968) 27.

[24] Olson, G. B., Bhadeshia, H. K. D. H. and Cohen, M., "Coupled Diffusional–Displacive Transformations", *Acta Metallurgica,* 37 (1989) 381–389.

[25] Hehemann, R. F., "The bainite transformation", Phase Transformations, eds H. I. Aaronson and V. F. Zackay, ASM (1970) 397–432.

[26] Bhadeshia, H. K. D. H. and Edmonds, D. V., "The mechanism of the bainite reaction in steels", *Acta Metall.* 28 (1980) 1265–1273.

[27] Bhadeshia, H. K. D. H., "Solute-drag, kinetics and the mechanism of the bainite transformation", Phase trans. in ferrous alloys, eds A R Marder & J I Goldstein, TMS–AIME, (1984) 335–340.

[28] Bhadeshia, H. K. D. H. and Christian, J. W., "The bainite reaction in steels", *Metallurgical Transactions A,* 21A (1990) 767–797.

[29] Christian, J. W., *Theory of Transformations in Metals and Alloys*, Part II, 3rd edition, Pergamon Press, Oxford, pp. 1089-1181, 2003.

[30] Peet, M., Babu, S. S., Miller, M. K. and Bhadeshia, H. K. D. H., "Three-Dimensional Atom Probe Analysis of Carbon Distribution in Low-Temperature Bainite", *Scripta Materialia* 50, pp. 1277-1281, 2004.

[31] Bhadeshia, H. K. D. H., "Large Chunks of Very Strong Steel", *Millenium Steel,* 5, pp. 25-28, 2004.

[32] Garcia-Mateo, C., Caballero, F. G. and Bhadeshia, H. K. D. H., "Acceleration of Low-Temperature Bainite", *ISIJ International,* 43, pp. 1821-1825, 2003.

[33] Hammond, R. I., Proud, W. G., "Does the pressure-induced phase transition occur for low-alloy steels", *Proceedings of The Royal Society of London*, A460, pp. 2959-2974, 2004.

[34] Crowther, D. and Brown, P. M., private communication, 2004.

[35] Brown, P. M. and Baxter, D. P., "Hyper–strength bainitic steels", Materials Science and Technology 2004, New Orleans, Louisiana, (2004) 433–438.